minerals

MDPI

Article

Implications for Metallogenesis and Tectonic Evolution of Ore-Hosting Granodiorite Porphyry in the Tongkuangyu Cu Deposit, North China Craton: Evidence from Geochemistry, Zircon U-Pb Chronology, and Hf Isotopes

Jungang Sun [1,2,*], Ting Liang [1], Hongying Li [3], Kun Yan [4], Yinyin Chao [2] and Zhanbin Wang [2]

[1] College of Earth Science and Resourses, Chang'an University, Xi'an 710054, China; liangt@chd.edu.cn
[2] Xi'an Center of Mineral Resources Survey, China Geological Survey, Xi'an 710100, China; cyy21618@outlook.com (Y.C.); keroleny@163.com (Z.W.)
[3] Institute of Mineral Resources, Chinese Academy of Geological Sciences, Beijing 100037, China; lihongy@163.com
[4] Yantai Center of Coastal Geological Survey, China Geological Survey, Yantai 264000, China; 18615978202@163.com
* Correspondence: jungangsun2019@163.com

Abstract: The Tongkuangyu copper deposit in Zhongtiaoshan at the southern margin of the North China Craton is one of the oldest porphyry Cu deposits in the world and its metallogenesis and tectonic evolution have been debated. Here, porphyritic intrusion geochemical and geochronological data are reported to identify the diagenetic age, mineralization, tectonic setting, and evolution of the deposit. Geochemical data show that granodiorite porphyry is a peraluminous rock, with low concentrations of Fe (~3.99%) and Ti (~0.29%) and high concentrations of alkali (~6.13%) and high Al (~15.42%) and Mg numbers (~51). The rocks show comparative enrichment of Na, K, and Mg; higher La/Yb ratios, no significant Eu anomaly, and obvious Nb–Ta–Ti negative anomaly, showing similar geochemical characteristics to Archean TTG and sanukitoid. ΣREE vary greatly, ranging from 33.47×10^{-6} to 277.81×10^{-6} (average 137.09×10^{-6}). The characteristics of REE show obvious fractionation of LREE and HREE, enrichment of LREE, and depletion of HREE. Some of the LREE (La and Ce) and LILE (K, Rb, and Ba) are enriched, but some of the LILE (Th and U) are depleted. In addition, some of the HFSE (Nb, Ta, P, and Ti) are depleted while some (Zr and Hf) are enriched. High precision LA–MC–ICP MS zircon U–Pb dating yield concordant ages of 2159 ± 19 Ma, which is broadly coeval with ore formation (~2.1 Ga) in the area. Zircon $\varepsilon_{Hf}(t)$ values range from −3.8 to 1.13, with a model age of 2778 to 2959 Ma, indicating that the formation of porphyry is related to the partial melting of Archean crust (~2.7 Ga) with a minor amount of mantle material added. Tongkuangyu granodiorite porphyry formed in the tectonic setting of the post-orogenic extension in the Paleoproterozoic, and Tongkuangyu Cu deposit may be related to the extension of the North China Craton in the Paleoproterozoic.

Keywords: granodiorite porphyry; geochemistry; U-Pb dating; Hf isotopes; Zhongtiaoshan; North China Craton

Citation: Sun, J.; Liang, T.; Li, H.; Yan, K.; Chao, Y.; Wang, Z. Implications for Metallogenesis and Tectonic Evolution of Ore-Hosting Granodiorite Porphyry in the Tongkuangyu Cu Deposit, North China Craton: Evidence from Geochemistry, Zircon U-Pb Chronology, and Hf Isotopes. *Minerals* **2022**, *12*, 273. https://doi.org/10.3390/min12020273

Academic Editors: Yong Lai and Maria Boni

Received: 27 December 2021
Accepted: 17 February 2022
Published: 21 February 2022

1. Introduction

The Zhongtiaoshan, extending in the NW–SE direction, is one of the most important Cu metallogenic belts in China and is located in southern margin of the North China Craton. The types of Cu deposits vary in this region and include porphyry-type (Tongkuangyu Cu deposit), sedimentary metamorphic-hydrothermal superimposed stratabound type (Hujiayu Cu deposit and Bizigou Cu deposit), metamorphic Cu-bearing shale type (Henglingguan Cu deposit), metamorphic hydrothermal type (Luojiahe Cu deposit), and hydrothermal vein type (Lujiaping Cu deposit). More than 20 Cu deposits and about 4 million tons

of Cu reserves have been found here. As a superlarge Cu deposit, Tongkuangyu Cu deposit has reserves of 2.8 million tons of copper (with an average grade of 0.6%) and minor amounts of gold, molybdenum, and cobalt [1].

The genetic type of Tongkuangyu Cu deposit has been debated since its discovery. Some researchers concluded that the mineralization was hosted in volcanic and subvolcanic rocks and was genetically linked to the porphyry intrusion [2–8]. However, others argued that the host rocks are sedimentary in origin and the mineralization is unrelated to the porphyry intrusion [9–12]. Debate arises because of a poor understanding of the magma nature, source, and mineralizing capacity of ore-forming porphyry. Limited by testing instruments and methods in early research, measured diagenetic ages vary greatly. In addition, previous studies mainly focused on the petrogenic age and regional tectonic evolution [1]. There are few studies on the geochemical characteristics of the ore-forming porphyry, and those that have been conducted lack comparisons with the hosted rock. Ensuring the origin of the Cu mineralization and providing new constraints for Paleoproterozoic tectonic evolution in the North China Craton, LA-ICP-MS zircon U-Pb isotopic dating and Lu-Hf isotopes of porphyry are presented to discuss the age, origin, and relationship of granites, which is useful for the further division of the mineralization stage and ore-forming material source.

In this paper, we study the major and trace elements of granite porphyries, U-Pb, and in-situ Lu–Hf of zircon by MC-LA-ICPMS, after which we can discuss the formation age of the porphyry, the magma source, the petrogenesis, and the possible significance of the tectonic evolution and Cu mineralization.

2. Regional Geology

2.1. Tectonic Framework

Tongkuangyu is located in the Zhongtiaoshan region, which lies on the southern margin of the central North China Craton (Figure 1A). The tectonic history of this region is poorly understood, but some tectonic thermal events have been recognized, including the Jiangxian movement and Zhongtiao orogenesis. The Jiangxian movement is marked by angular unconformity between the Jiangxian Group and the Zhongtiao Group, and its time is roughly constrained to 2100–2060 Ma [13]. The Zhongtiao orogenesis is characterized by angular unconformity between the Zhongtiao Group and the Danshanshi Group, and its time is ~1.9–1.85 Ga [1,14], which was caused by the collision of the eastern and western North China blocks (~1.85 Ga) [15,16]. After that, crustal thickening (1843–1817 Ma) [17] and emplacement of syncollisional (~1832 Ma) and postcollisional (1815–1790 Ma) granite occurred in the North China block [18,19].

In addition, the Zhongtiao orogenesis is the most important metamorphic phase, from greenschist to amphibolites facies, and peak metamorphism is achieved at ~1.9 to 1.85 Ga, which superimposed early fabrics and textures on the Jiangxian Group and Zhongtiao Group [13,20]. The above basically determine the current tectonic framework of the Zhongtiaoshan region.

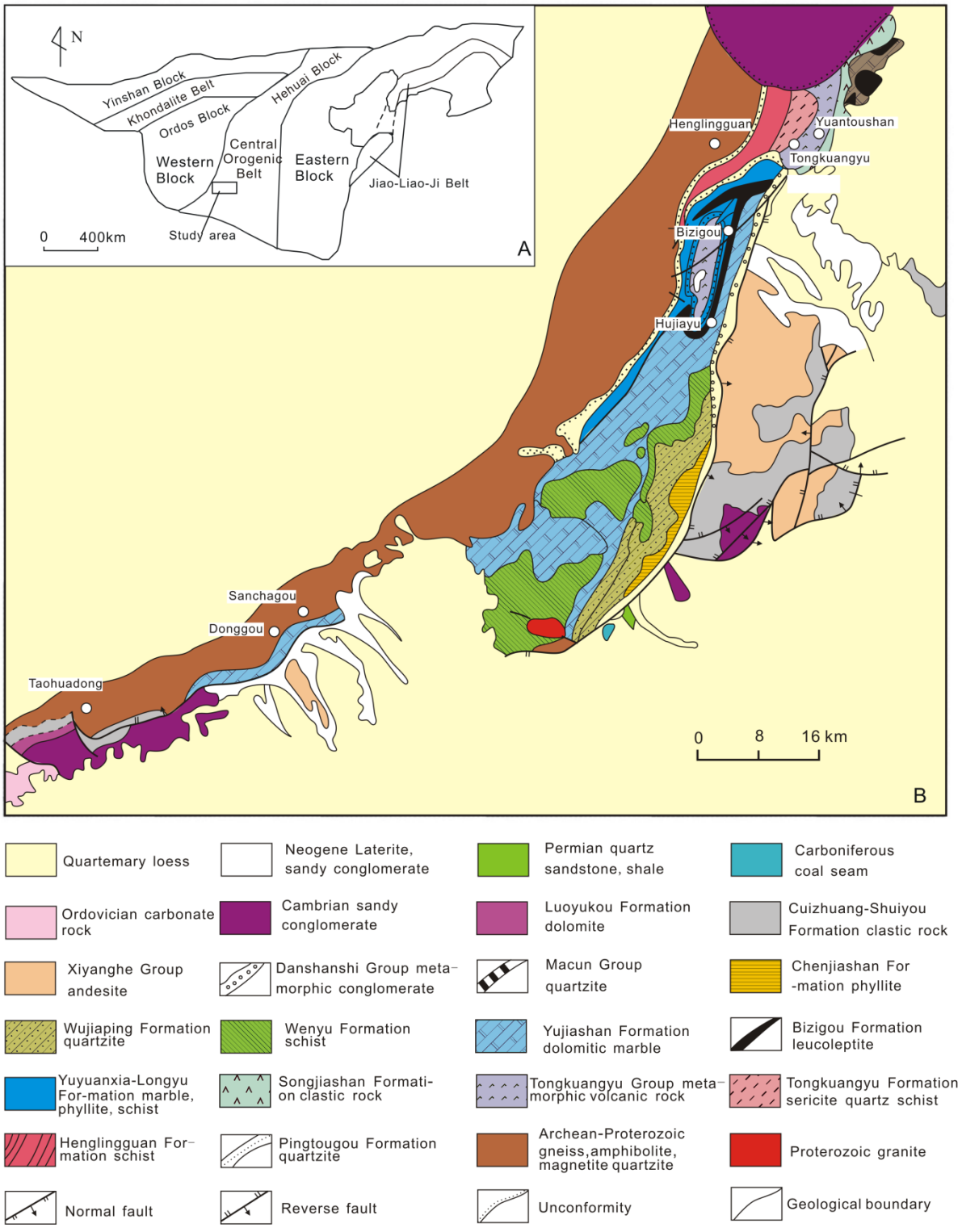

Figure 1. Simplified geotectonic map of study area (**A**) and Regional geological map of Zhongtiaoshan (**B**) (modified after CGGCDZM, 1978 [1]).

2.2. Stratigraphy

Various types of Precambrian rock units (Neoarchean to Paleoproterozoic) are exposed in Zhongtiaoshan area, including the Sushui Complex, the Jiangxian Group, the Zhongtiao Group, the Danshanshi Group, and the Xiyanghe Group (from oldest to youngest) (Figure 1B).

As the oldest complex in the Zhongtiaoshan region, the Sushui Complex consists of TTG gneisses of the Neoarchean (~2.7–2.5 Ga) [21–25], metamorphosed supracrustal rocks of the Paleoproterozoic (~2.5–2.3 Ga), and granitic intrusions from the Neoarchean to Paleoproterozoic [22,23].

The early Paleoproterozoic Jiangxian Group overlies the Sushui Complex with angular unconformity, which consists of metasedimentary and metavolcanic rocks. Lithology includes silty and argillaceous schist in the lower Jiangxian Group (Henglingguan sub-group), quartz-sericite schist, biotite schist, and metarhyolite in the upper Jiangxian Group (Tongkuangyu sub-group). Although their stratigraphic relationship is unclear, they are interpreted as being of volcanic and volcaniclastic origin, which has been dated between ~2.5 and 2.2 Ga [8,14,20,26].

The middle Paleoproterozoic Zhongtiao Group unconformably overlies the Jiangxian Group and is composed of clastic sediments, carbonate rocks, and minor basic-to-intermediate volcanic rocks, with time limits of 2110–2060 Ma [14,20,27–29]. This sequence is interpreted to as being deposited in the back-arc basin in the eastern North China block during the closure of the ocean basin between the eastern and western North China block [27], but the nature of the subduction is still controversial [30,31].

The late Paleoproterozoic Danshan Group unconformably overlies the Zhongtiao Group and consists of metaconglomerate and sandstone, which is typical molasse formation. The maximum sedimentary age is about 1848 Ma [28], which indicates the end of the cratonization of the North China craton [14,32].

The late Paleoproterozoic Xiyanghe Group overlies the Danshanshi Group with angular unconformity, which is composed of bimodal volcanic rocks erupted between 1.81 and 1.76 Ga in the rifts of Zhongtiaoshan region [8,33].

2.3. Magmatic Rock

Paleoproterozoic magmatic events can be divided into the pre-Jiangxian, Jiangxian, Zhongtiao, and Xiyanghe periods [7]. Magmatic activity of the pre-Jiangxian period is related to various intrusions of granitoid [34]. The Jiangxian period is the peak period of volcanic–magmatic activity, during which magmatic activities were relatively intense and frequent and volcanic eruptions occurred with small-scale intrusions, resulting in the accumulation of a series of bimodal volcanic rocks characterized by potassic mafic volcanic rocks, quartz porphyries, potassic rhyolites, and quartz crystal tuffs [32]. The Zhongtiao period consists of early basic magmatism and late acid magmatism [35]. The magmatism of the Xiyanghe period is characterized by the eruption of basaltic andesite–andesite and emplacement of mafic dikes, forming a set of very thick intermediate–basic volcanic rocks [34].

3. Deposit Geology and Petrography

3.1. Deposit Geology

The exposed rocks in the Tongkuangyu ore district mainly include schists of the Luotuofeng Formation and felsic porphyritic intrusive rocks. Schists mainly consist of quartzite, quartz-sericite schist, and metamorphic volcanic rock (Figure 2). Felsic porphyritic intrusive rocks include granodiorite and granodiorite porphyry. The main orebodies at Tongkuangyu are hosted by granodiorite porphyry, biotite schist, and quartz-sericite schist. The biotite schist was previously interpreted to be either a mafic volcanic or intrusive rock [1,36] or metapelite [37]. The quartz-sericite schist has previously been interpreted to be either a tuffaceous argillite [1], porphyroblastic mylonite [38], or metapelite [37]. In addition, these schists and granodiorite porphyry were crosscut by diabase dikes locally.

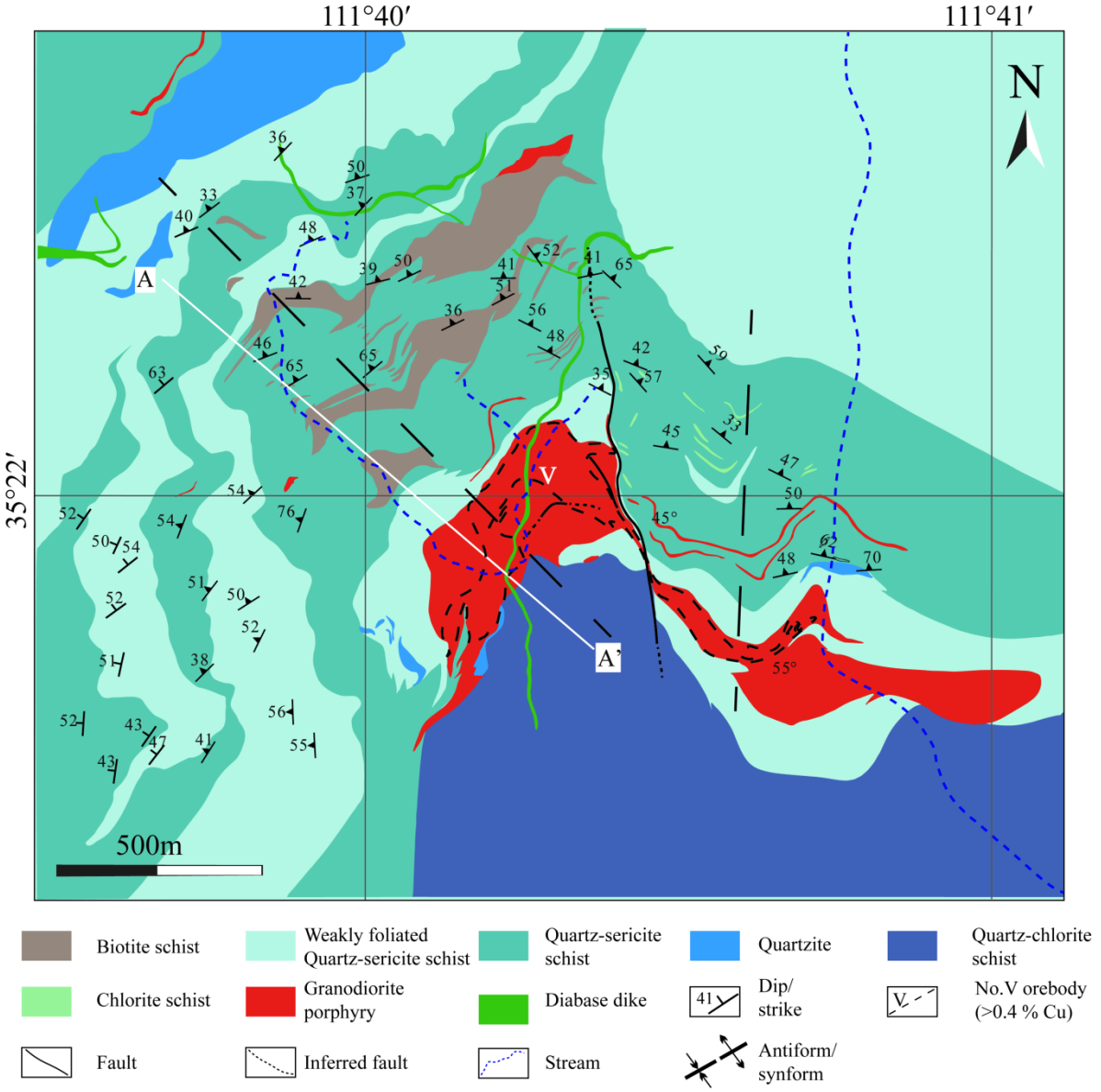

Figure 2. Simplified geologic map of the Tongkuangyu Cu deposit (modified after 214 Geological Group in Zhongtiaoshan in Shanxi Province, unpub. report, 1956; Meng et al., 2020 [8]).

Cu mineralization is restricted to Luotuofeng Formation and granodiorite porphyry intrusions (Figure 3), and occurs in five main orebodies (Nos. 1–5). Among them, No.4 and 5 orebody are the largest in scale, with reserves accounting for more than 85% of the whole deposit, and are hosted by granodiorite porphyry. No.1, 2, and 3 ore bodies are small in scale and mainly occur in biotite schist. No.5 ore body starts from Shuiyaogou in the east to Heiyingou in the west, with a length of 1100 m along the strike. The controlled lowest level is 575–700 m, and it continues to extend downward. Ore body pitches to NE and occurs as flatted lenses with a thickness of 185 m at the center and 6–28–61 m at edge. No.4 orebody, which is located above No.5 orebody, is a concealed orebody 840 m along the strike and more than 830 m along the dip with angle of about 40° that has a thickness of 30–218 m, pitches to the SW at an angle of 22°, and occurs as flatted lenses with a thick center and thin edge.

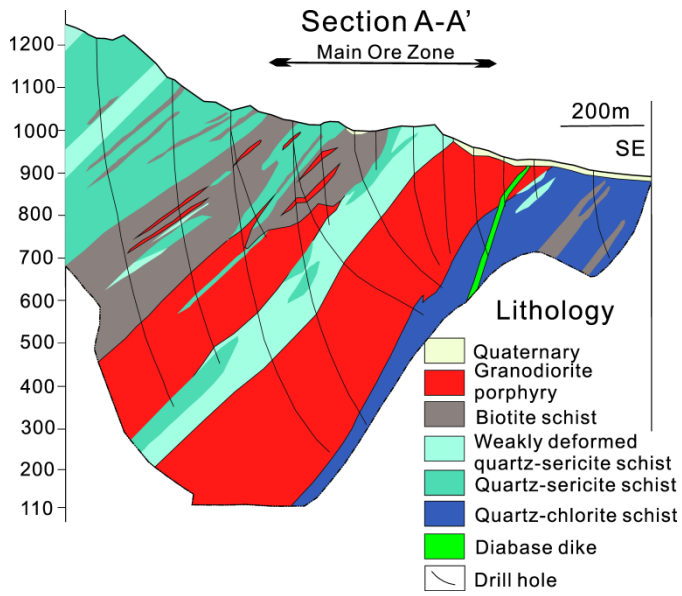

Figure 3. Geological section of the main ore veins (modified after 214 Geological Group in Zhongtiaoshan in Shanxi Province, unpub. report, 1956; Meng et al., 2020 [8]).

The host rocks of the Tongkuangyu Cu deposit display various types of hydrothermal alteration, but the nature and distribution of this alteration has been obscured by later metamorphism and overprinting by late-stage hydrothermal fluids [1]. Sun et al. (2014) [4] identified sericite and albite alteration overprinted by ore-associated biotite ± K–feldspar alteration followed by late-stage chlorite and minor carbonate alteration. In this study, we briefly redescribe the distribution and characteristics of secondary minerals. Potash feldspar mainly occurs in mineralized granodiorite porphyry, which replaces feldspar minerals and sometimes occurs as a quartz–potassic feldspar vein. Biotite occurs in almost all rocks. Within granodiorite porphyry and meta–tuff, biotite replaces primary mafic minerals. Within biotite schist and sericite–quartz schists, biotite forms major minerals with sericite and quartz and sometimes occurs as veinlets. Within granodiorite porphyry and meta–tuff, chlorite often replaces biotite, which is sometimes completely replaced and presents the pseudomorph of original minerals. Sericite occurs in almost all rocks. Within the sericite–quartz schist, sericite usually occurs with quartz. Within granodiorite porphyry and meta–tuff, sericite often occurs in matrix with quartz or replaces the feldspar phenocrysts. With obvious alteration zoning, there is a K–silicate zone, a propylitic zone, a quartz–sericite zone and a kaolinized zone (from inner to outer). The characteristics of the altered zones and their relationship with the mineralized zones in Tongkuangyu Cu deposit are shown in Figure 4.

The mineralization of Tongkuangyu Cu deposit was studied by previous research [1,4]. In this study, the mineralization of this deposit is redivided in detail. Ore bodies are mainly composed of veinlet-disseminated metallic sulfide in the early stages and sulfide-bearing quartz (–carbonate) veins in the late stages. Ore minerals include chalcopyrite, pyrite, bornite, molybdenite, magnetite, and a little chalcocite. Granodiorite porphyry is well mineralized and is dominated by disseminated chalcopyrite and pyrite. The ore body is mainly disseminated or a veinlet-like metal sulfide vein, which is usually consistent with foliation of wall rock and often crosscut by a later sulfide-bearing quartz (carbonate) vein. Similarly, mineralized biotite schists are mainly composed of disseminated/vein–like metal sulfides and chalcopyrite/pyrite/quartz/carbonate veins. The mineralization in the Tongkuangyu Cu deposit shows obvious zonation, which consists of, respectively, molybdenite zone → molybdenite + chalcopyrite + bornite zone → chalcopyrite + pyrite zone → pyrite zone (from inner to outer). According to the intercalated relationship between different veins, the mineralization stage of the Tongkuangyu Cu deposit can be

divided into a quartz–potash feldspar stage, a quartz–sulfide stage, a quartz–carbonate stage, and a carbonate stage. The different vein types and their intercalated relationship in Tongkuangyu Cu deposit are shown in Figure 5.

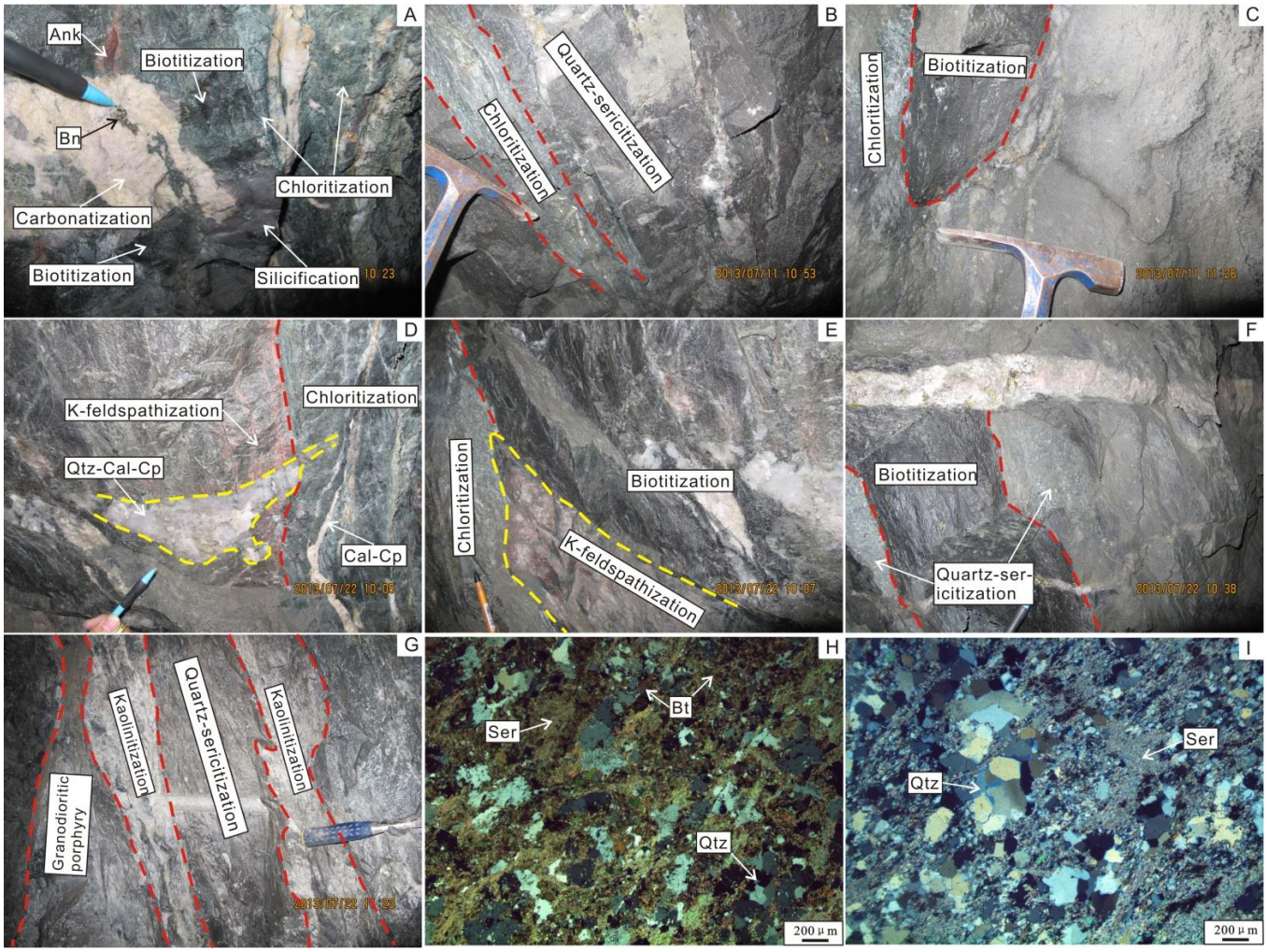

Figure 4. Different alteration types in the Tongkuangyu deposit. (**A**) Chloritization, biotitization, silication, and carbonatization in biotite schist (Sample 1381, No. 5147 tunnel of No. V orebody on 690-m level). (**B**) Chloritization and quartz–sericitization in quartz–sericite schist (Sample 1569, No. 4143 tunnel of No. IV orebody on 530-m level). (**C**) Chloritization and biotitization in biotite schist (Sample 1604, No. 4143 tunnel of No. IV orebody on 530-m level). (**D**) K–feldsparization and chloritization crosscut by quartz–calcite–chalcopyrite vein. Quartz–calcite–chalcopyrite vein cut by calcite–chalcopyrite vein within chloritization zone (Sample 2599, No. 5147 tunnel of No. V orebody on 690-m level). (**E**) Chloritization, biotitization and K feldspathization in biotite schist (Sample 2603, No. 5147 tunnel of No. V orebody on 690-m level). (**F**) Quartz–sericitization along biotitization zone (Sample 2633, No. 4143 tunnel of No. IV orebody on 530-m level). (**G**) Quartz–sericitization and kaolinizitation in the contact zone between granodiorite porphyry and quartz–sericite schist (Sample 2643, No. 4143 tunnel of No. IV orebody on 530-m level). (**H**) Biotite schist (sample 5147–3–2); cross-polarized light. (**I**) Quartz–sericite schist (sample 5147–20); cross-polarized light. Abbreviations: Qtz: quartz; Bt: biotite; Ser: sericite; and Bn: bornite.

Figure 5. Vein types and their relationships in Tongkuangyu deposit. (**A**) Quartz–chalcopyrite–pyrite vein cutting quartz–K feldspar–chalcopyrite–pyrite vein, all crosscut by later calcite–chalcopyrite–pyrite vein (Sample 263–14, No. 263 drilling of No. V orebody). (**B**) Late quartz–magnetite vein cutting barren quartz vein (Sample 256–10, No. 256 drilling of No. V orebody). (**C**) Quartz–chalcopyrite–pyrite vein cutting veinlet-disseminated chalcopyrite ± pyrite in granodiorite porphyry (Sample 0629, No. 041 drilling of No. IV orebody). (**D**) Quartz–chalcopyrite–pyrite vein crosscut by quartz–calcite–chalcopyrite–pyrite–specularite vein (Sample 4s'–19, No. 041 drilling of No. IV orebody). (**E**) Quartz–chalcopyrite–pyrite vein crosscut by quartz–calcite–chalcopyrite–pyrite vein (Sample 0653, No. 041 drilling of No. IV orebody). (**F**) Quartz–calcite–chalcopyrite–bornite vein cutting quartz–chalcopyrite–pyrite vein (Sample 1387, No. 5147 tunnel of No. V orebody on 690-m level). (**G**) Calcite–chalcopyrite–pyrite vein cutting quartz–calcite–chalcopyrite–bornite (Sample 1484, No. 5147 tunnel of No. V orebody on 690-m level). (**H**) Late calcite vein cutting K–feldsparization, biotitization and silication (Sample 2884, No. 263 drilling of No. V orebody). (**I**) K–feldsparization, biotitization, sericitization, and silication beside quartz–chalcopyrite vein (Sample 2871, No. 263 drilling of No. V orebody). Abbreviations: Qtz: quartz; Cp: chalcopyrite; Py: pyrite; Kfs: K–feldspar; Cal: calcite; Mt: magnetite; Pl: plagioclase; Spe: specularite; Bn: bornite; Bt: biotite; and Ser: sericite.

3.2. Petrographic Characteristics

Granodiorite porphyry is enclosed in quartz–sericite schist and biotite schist, and only identified in drill cores and underground tunnels. Rocks are grey black and grey, with a fine-grained porphyritic texture and a massive structure (Figure 6A–C). The phenocryst content is about 30% to 40%, and mainly consists of quartz, plagioclase, K–feldspar, and biotite. The matrix content is about 60% to 70% and is mainly composed of quartz, sericite, and biotite (Figure 6D–I). Accessory minerals are rutile, apatite (Figure 6G,I), zircon (Figure 6E), magnetite, and ilmenite. Quartzes mostly have obvious melting corrosion structures in the shapes of bay-like and round. Plagioclases are usually in the shape of platy and flake or

subhedral and euhedral with a polysynthetic twin and zonal structure. Sericitization often occurs on the surface, and sometimes carbonation can be seen. K–feldspars are usually in the shape of platy and flake or subhedral and euhedral with a Carlsbad twin, grid twin, and zonal structure, and sericitization and clayization often occur on the surface. Biotites are usually in the shape of platy, flake, and long strip or subhedral and euhedral with perfect cleavage and obvious pleochroism (light brown to yellowish brown). Chloritization often occurs along the cleavage or mineral particles' edge and some of them are even completely replaced by chlorite, showing the pseudomorph of chlorite. Apatites are long columnar and granular in shape and often contain or are contained by other minerals, but most of them coexist with biotite. Chlorites are altered mineral, which often replace biotite along mineral particle edges or cleavages. Zircons are long columnar and occasionally cross-cut by later veins. Rutiles are granular and platy and are often contained in biotite, causing an obvious metasomatic reaction.

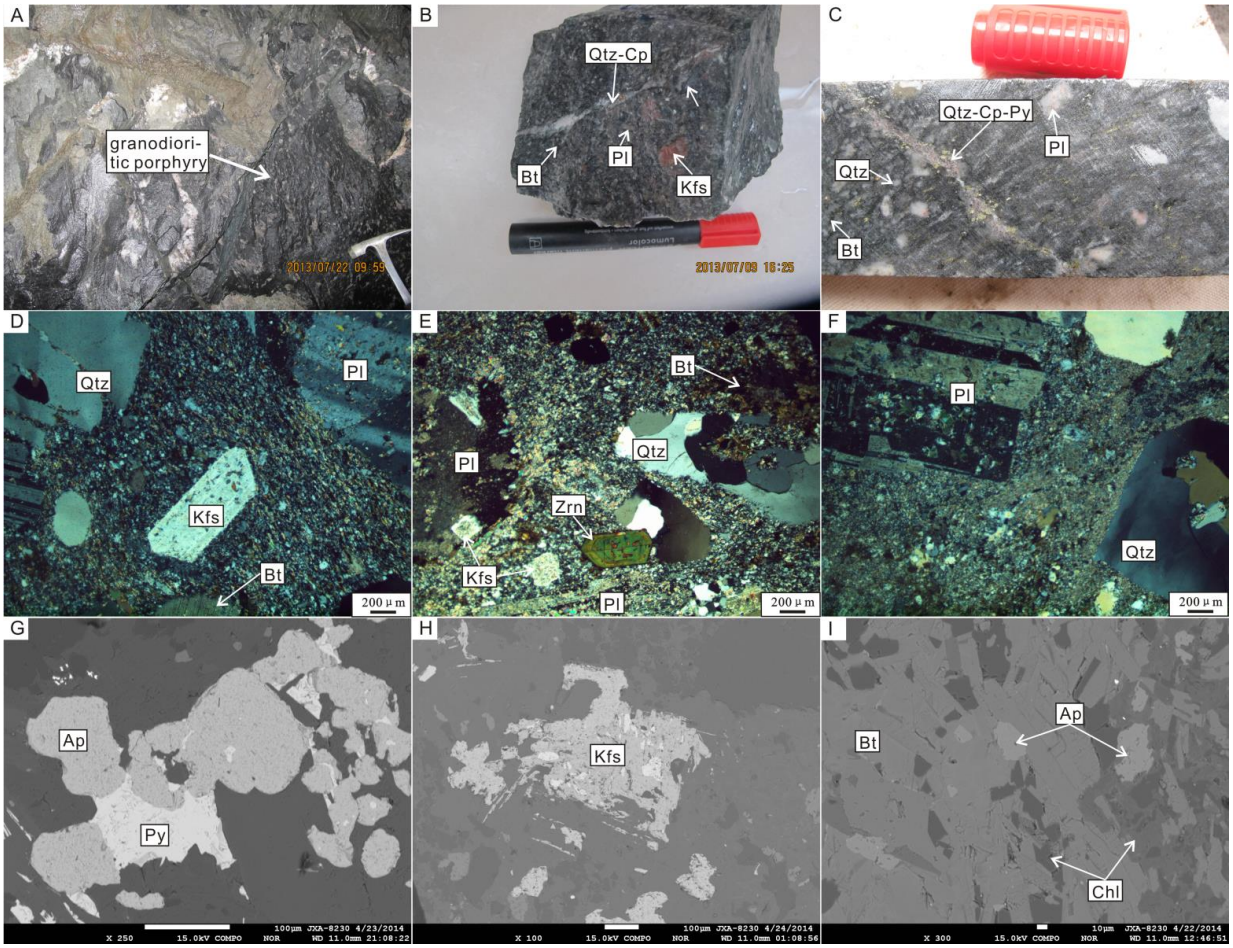

Figure 6. Representative photographs and photomicrographs of granodiorite porphyry from Tongkuangyu. (**A**) Biotite schist intruded by granodiorite porphyry (Sample 2596, No. 5147 tunnel of No. V orebody on 690-m level). (**B**) The granodiorite porphyry is cross-cut by quartz– chalcopyrite–pyrite vein (Sample D1, No. 5141 tunnel of No. V orebody on 540-m level). (**C**) Quartz–chalcopyrite–pyrite vein cutting veinlet-disseminated chalcopyrite–pyrite in granodiorite porphyry (Sample 263–3, No. 263 drilling of No. V orebody). (**D**–**F**) Granodiorite porphyry (sample D4, D5, and D6); cross–polarized light; No. 5141 tunnel of No. V orebody on 540-m level. (**G**) Apatite intergrown with pyrite in granodiorite porphyry (sample 5s–1); baskscattered electron (BSE) image. (**H**) Crystals of feldspar in granodiorite porphyry (sample 5s–13); BSE. (**I**) Apatite, biotite, and chlorite in granodiorite porphyry (sample 5s–26); BSE. Abbreviations: Qtz: quartz; Cp: chalcopyrite; Py: pyrite; Kfs: K–feldspar; Bt: biotite; Zrn: zircon; Ap: apatite; and Chl: chlorite.

4. Analytical Method

4.1. Sampling

Five granodiorite porphyry samples (D1, D4 from No.5141 tunnel of level 540 m; 5147–19 from No.5147 tunnel of level 690 m; 4s–2,4s–5 from drill core No.4S125) were collected for bulk–rock major and trace elements analysis. One granodiorite porphyry sample (D1 from No.5141 tunnel of level 540 m) was conducted by zircon laser ablation MC–ICP–MS analysis. One granodiorite porphyry sample was analyzed by multi–collector laser ablation MC-ICP-MS for Lu–Hf. The sample locations are summarized in Table 1.

Table 1. Sample locations of Tongkuangyu granodiorite porphyry.

Sample No.	Location	
	Tunnel No.	Drilling No.
D1	5141 (level 540 m)	
D4	5141 (level 540 m)	
5147-19	5147 (level 690 m)	
4s-2		4s125 (level 3.6 m)
4s-5		4s125 (level 5.1 m)

4.2. Bulk-Rock Major and Trace Elements

The major and trace elements of bulk-rock were analyzed in the National Research Center of Geoanalysis (China). The samples were ground to below 200 mesh with a hammer and agate mortar. The prepared samples were mixed with a lithium metaborate/lithium tetraborate reagent and lithium nitrate was used as an oxidant. The mixture was then poured into a platinum mold to form a fused disk for X-ray fluorescence (XRF) analysis of the major elements. Loss on ignition (LOI) of each sample at 1000 °C was measured and element concentration was calculated based on the results of both analyses. Rare earth and trace elements were analyzed by inductively coupled plasma mass spectrometry (ICP-MS). Prepared samples were mixed with lithium metaborate/lithium tetraborate flux and fused in a furnace at 1025 °C. Before analysis, the resulting melts were cooled and dissolved in a mixture of nitric acid, hydrochloric acid, and hydrofluoric acid. For major elements, the testing instrument type was PW4400 and analysis precision was 1% to 5%, and for rare earth and trace elements it was X-series and 5% to 10%. Fe_2O_3 and FeO were separately analyzed by wet method.

4.3. Zircon U-Pb Dating

Zircon sorting work was completed in the Rock and Mineral Experimental Testing Center of Langfang Geological Surveying and Mapping Institute in Hebei Province. Zircon cathode photoluminescence (CL) photography was performed using a JXA–8100 electron probe at the Institute of Geology, Chinese Academy of Geological Sciences (CAGS). The zircon U–Pb dating was performed at the MC–ICP–MS laboratory of the Institute of Mineral Resources, CAGS, using a Finnigan Neptune type MC–ICP–MS and a Newwave UP213 laser ablation system. A spot size of laser beam was 25 μm, with a frequency of 10 Hz and energy density of 2.5 J/cm^2, and Helium gas was used as the carrier gas. Zircon international standard GJ1 was used as the external standard for dating, and U and Th mass fractions were corrected by zircon M127 as the external reference. Data were processed using ICP–MS–DataCal 4.3 [39] and zircon age harmonic diagram was obtained using Isoplot 4.15 program [40]. The detailed experimental testing process was given by Hou et al. (2009) [41].

4.4. Zircon Lu-Hf Isotopes

The zircon Lu–Hf isotope test was completed in the MC–ICP–MS laboratory of the Institute of Mineral Resources, CAGS. A Finnigan Neptune plasma mass spectrometer and a Newwave UP213 laser ablation system were used with a beam diameter of 50 μm,

carrier gas of He and ablation time of 27 s. The internationally accepted zircon standard GJ–1 was used as a reference, and the analysis point was same position as the zircon U–Pb dating point. For instrument operating conditions and detailed analysis procedure, refer to the reference by Hou et al. (2007) [42] and Wu et al. (2006) [43]. The parameters for calculating $\varepsilon_{Hf}(t)$ and mode age are as follows: $\lambda(^{176}Lu) = 1.867 \times 10^{-11}$ a^{-1} [44], $(^{176}Lu/^{177}Hf)_{CHUR} = 0.0332$, $(^{176}Hf/^{177}Hf)_{CHUR} = 0.282772$ [45], $(^{176}Lu/^{177}Hf)_{DM} = 0.0384$, $(^{176}Hf/^{177}Hf)_{DM} = 0.28325$ [46], and $(^{176}Lu/^{177}Hf)_{CC} = 0.015$ [47].

5. Results

5.1. Zircon U-Pb Geochronology

Zircons selected from Tongkuangyu granodiorite porphyry are mostly colorless and transparent and crystals are subhedral–euhedral with a particle size of 50 to 100 μm and length/width ratio of 2 to 3. Most of them are short to long columnar, and few are perfectly round. The crystal surface of the zircons is complete, straight, and smooth. The CL image (Figure 7) shows that most zircons have oscillatory zoning, with obvious core, mantle, and rim zoning. Th contents of zircons range from 1191 $\times 10^{-6}$ to 3616 $\times 10^{-6}$, U contents vary from 1976 $\times 10^{-6}$ to 6148 $\times 10^{-6}$, Th/U ratios change from 0.43 to 1.52 and all of them are greater than 0.4, suggesting a magmatic origin. A total of 11 valid points were obtained with $^{207}Pb/^{206}Pb$ ages ranging from 2121 to 2184 Ma (Table 2). Most of the data fall on and near the concordia line. The upper intercept age is 2180 ± 37 Ma (Figure 8A), and the weighted average age is 2159 ± 19 Ma (Figure 8B), which represents the diagenetic age of the Tongkuangyu ore-forming granodiorite porphyry.

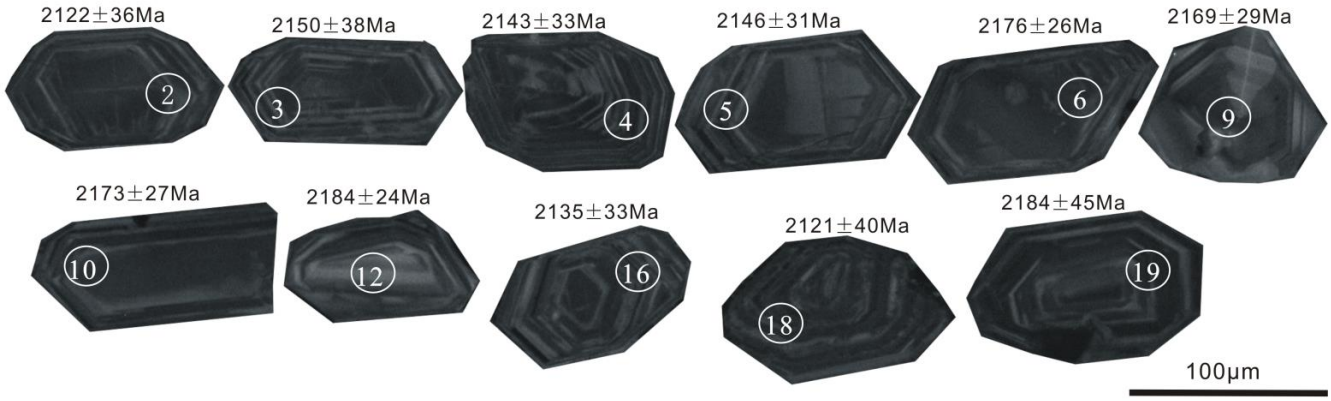

Figure 7. Zircon cathodoluminescence (CL) images of Tongkuangyu granodiorite porphyry.

Table 2. LA–ICP–MS zircon U–Pb data of Tongkuangyu granodiorite porphyry.

Sample No.	Th	U	Th/U	Isotope Ratio						Age(Ma)					
	(10^{-6})			$^{207}Pb/^{206}Pb$		$^{207}Pb/^{235}U$		$^{206}Pb/^{238}U$		$^{207}Pb/^{206}Pb$		$^{207}Pb/^{235}U$		$^{206}Pb/^{238}U$	
				Ratio	1σ	Ratio	1σ	Ratio	1σ	Age	1σ	Age	1σ	Age	1σ
D1.2	3616.4	5071.2	0.71312	0.13103	0.00272	6.45744	0.16000	0.35612	0.00742	2122	36	2040	22	1964	35
D1.3	2905.9	6148.3	0.47263	0.13383	0.00294	6.30404	0.17506	0.34019	0.00840	2150	38	2019	24	1888	40
D1.4	2226.8	5127.3	0.43431	0.13338	0.00250	7.00904	0.15356	0.38025	0.00719	2143	33	2113	19	2077	34
D1.5	2793.3	5377.5	0.51945	0.13357	0.00240	6.33486	0.14811	0.34259	0.00671	2146	31	2023	21	1899	32
D1.6	1750.2	4043.8	0.43283	0.13591	0.00210	6.96053	0.15115	0.37026	0.00714	2176	26	2106	19	2031	34
D1.9	3009.6	1976.1	1.52297	0.13527	0.00221	7.01250	0.14042	0.37702	0.00724	2169	29	2113	18	2062	34
D1.10	1191.1	2522.0	0.47229	0.13571	0.00211	7.38228	0.12564	0.39436	0.00548	2173	27	2159	15	2143	25
D1.12	2051.8	3296.9	0.62233	0.13657	0.00184	7.66763	0.12230	0.40684	0.00513	2184	24	2193	14	2200	24
D1.16	2508.9	3205.2	0.78275	0.13278	0.00251	6.09988	0.13558	0.33257	0.00336	2135	33	1990	19	1851	16
D1.18	1802.2	3176.6	0.56735	0.13175	0.00299	6.02383	0.17332	0.33081	0.00406	2121	40	1979	25	1842	20
D1.19	1279.8	2274.1	0.56277	0.13660	0.00354	7.09502	0.20799	0.37889	0.00598	2184	45	2123	26	2071	28

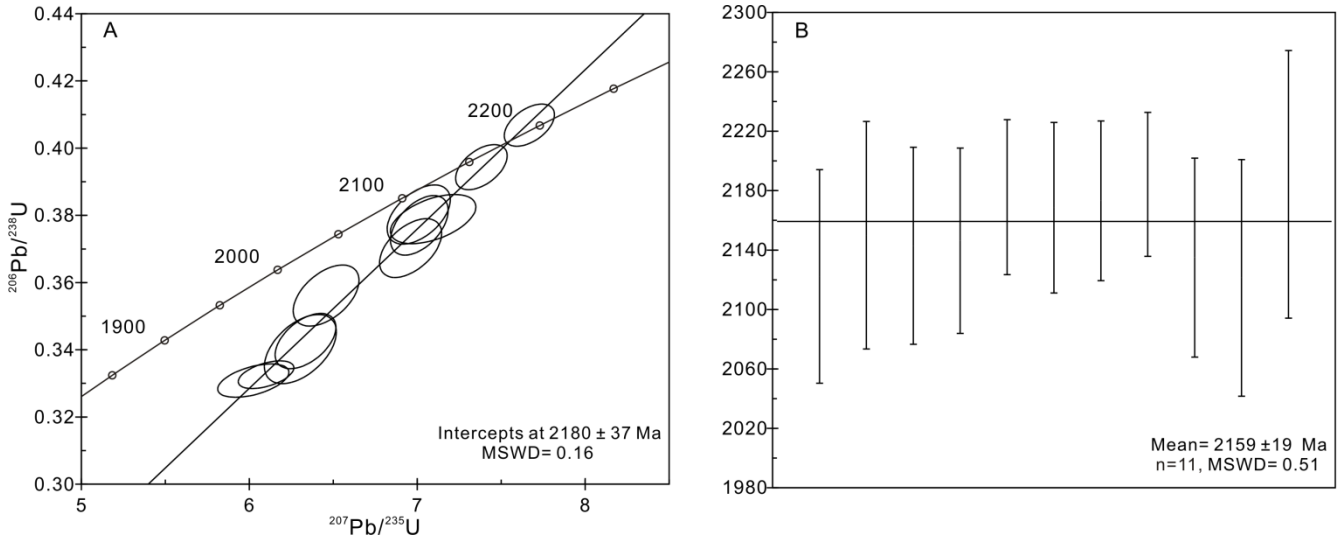

Figure 8. U-Pb Concordant diagram (**A**) and weighted average diagram (**B**) for Tongkuangyu granodiorite porphyry.

5.2. Rock Geochemistry

5.2.1. Major Compositions

The analysis results for major elements are shown in Table 3 (percentage after removal of loss on ignition), in which SiO_2 content is 65.84% to 70.61% (average 68.43%) and CaO content is 1.32% to 5.49% (average 2.89%). The contents of FeO^T and TiO_2 are relatively low, at 3.04% to 6.28% (average 3.99%), 0.23% to 0.41% (average 0.29%), respectively. The Mg index is high from 48 to 60 (average 51). The content of alkali is relatively high—Na_2O is 0.69% to 4.49% (average 2.31%), K_2O is 2.56% to 4.99% (average 3.81%), Na_2O/K_2O is 0.16 to 1.70, and total alkali is 4.89% to 7.66% (average 6.13%). The content of Al_2O_3 is 12.74% to 18.18% (average 15.42%), and aluminum saturation index A/CNK is 0.81 to 1.68 (average 1.21), which belongs to peraluminous rock. In the Nb/Y–Zr/TiO_2 discrimination diagram (Figure 9A), four samples plot in the granodiorite and one sample plots in the syenite field. In the K_2O–SiO_2 diagram (Figure 9B), three samples fall in the field of high-K calc-alkaline series, one falls in shoshonitic series, and one falls in calc-alkaline series.

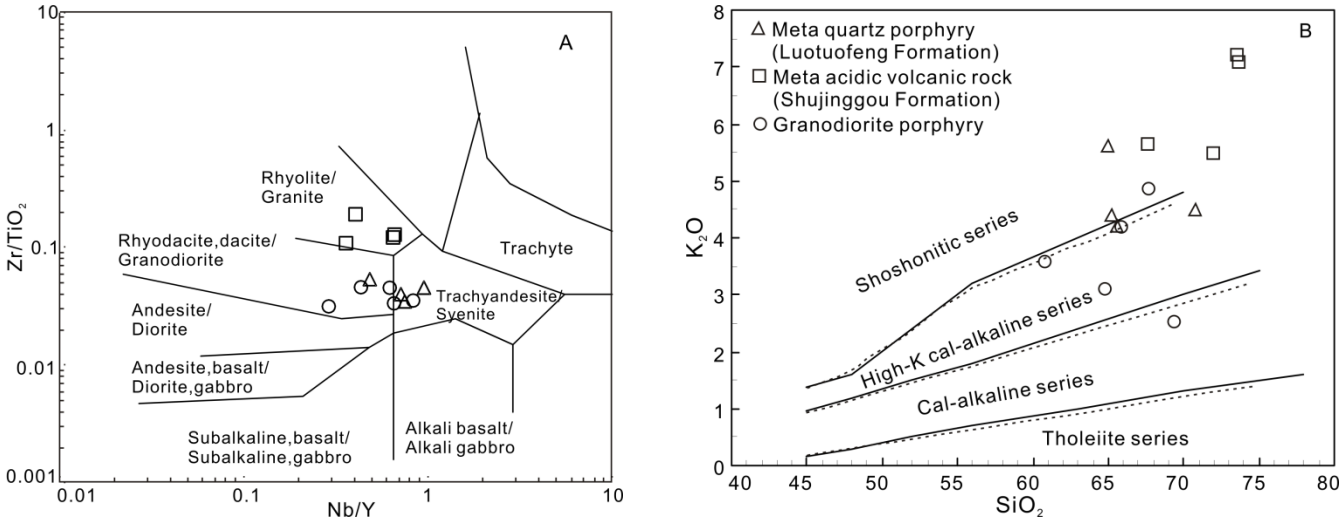

Figure 9. Nb/Y vs. Zr/TiO_2 (**A**) and SiO_2 vs. K_2O (**B**) diagrams for the major rock types from the Tongkuangyu district (after Winchester and Floyd, 1977 [48]; Middlemost, 1985, 1994 [49,50]; Peccerillo et al., 1976 [51]; andregional rock data from Yang et al., 2015 [52]).

Table 3. Whole rock major and trace element compositions of Tongkuangyu granodiorite porphyry.

Sample No.	D1	D4	5147-19	4S-2	4S-5
SiO_2 (%)	69.46	70.61	65.84	66.60	69.63
TiO_2	0.23	0.24	0.41	0.26	0.32
Al_2O_3	14.47	15.55	18.18	12.74	16.15
Fe_2O_3	1.79	1.65	1.57	2.41	2.01
FeO	1.95	1.59	1.81	4.31	2.23
MnO	0.06	0.02	0.02	0.07	0.02
MgO	2.97	1.57	2.09	3.10	2.07
CaO	3.83	1.71	2.11	5.49	1.32
Na_2O	0.69	4.36	4.49	0.94	1.09
K_2O	4.41	2.56	3.17	3.95	4.99
P_2O_5	0.14	0.14	0.30	0.13	0.19
LOI	2.68	1.60	1.49	2.62	2.60
Mg	59.78	47.62	53.69	46.04	47.71
Na_2O/K_2O	0.16	1.7	1.42	0.24	0.22
$Na_2O + K_2O$	5.09	6.93	7.66	4.89	6.08
A/NK	2.46	1.56	1.68	2.19	2.25
A/CNK	1.13	1.19	1.24	0.81	1.68
La (ppm)	6.69	24.3	61.2	33.5	26
Ce	12.8	46	119	64.6	49.2
Pr	1.56	5.27	14.1	7.8	5.52
Nd	6.18	18.6	52.1	29.3	19.7
Sm	1.15	2.65	8.49	5.3	3.03
Eu	0.29	1.07	2.67	1.51	0.79
Gd	1.29	2.53	7.57	5.2	2.76
Tb	0.18	0.35	1.1	0.71	0.33
Dy	0.95	1.89	5.65	3.88	1.88
Ho	0.22	0.37	1.01	0.69	0.35
Er	0.73	1.03	2.44	1.82	1
Tm	0.14	0.14	0.32	0.29	0.15
Yb	1.07	1	1.93	2.05	0.93
Lu	0.22	0.13	0.23	0.43	0.14
Y	6.77	10.4	25.8	17.2	9.76
Hf	2.72	3.46	5.22	2.53	3.15
Ta	0.6	0.69	1.05	0.51	0.6
Pb	0.96	1.55	1.42	1.78	1.57
Th	4.28	4.56	4.45	3.9	4.2
U	1.12	1.91	1.4	0.86	0.7
Sc	4.68	4.56	5.39	6.13	6.21
V	34.6	27.8	27.2	41.4	51.6
Cr	21.4	8.6	2.78	8.1	9.77
Co	9.44	8.62	7.32	32.9	15.2
Cu	1548	47	240	10811	1697
Mo	0.13	0.2	0.57	2.61	0.14
Zn	11.9	7.2	5.22	7.79	6.26
Rb	120	74.5	81.4	185	123
Sr	56.1	239	168	40.1	41.2
Zr	84.5	114	192	85.5	110
Nb	5.54	6.35	11	4.9	6.29
Ba	779	587	938	300	1157
Ni	18.3	7.39	8.15	24.8	8.68
As	0.92	0.94	0.93	0.68	0.75
Sb	0.11	0.13	0.13	0.08	0.08
W	2.83	1.64	5.64	1.6	13.8
Sn	1.24	1.52	1.88	1.8	1.7
Ga	15.8	15	21.1	10.7	18.9
Cs	1.11	1.11	1	1.42	1.23
Ag	0.1	0.02	0.03	0.4	0.06

Table 3. *Cont.*

Sample No.	D1	D4	5147-19	4S-2	4S-5
Au	45.9	1.08	2.29	203	17.8
ΣREE	33.47	105.33	277.81	157.08	111.78
LREE	28.67	97.89	257.56	142.01	104.24
HREE	4.8	7.44	20.25	15.07	7.54
LREE/HREE	5.97	13.16	12.72	9.42	13.82
Nb/Ta	9.23	9.2	10.48	9.61	10.48
Zr/Hf	31.07	32.95	36.78	33.79	34.92
La/Yb	6.25	24.3	31.71	16.34	27.96
δEu	0.72	1.25	1	0.87	0.82
δCe	0.94	0.95	0.96	0.94	0.96

5.2.2. Trace Elements Compositions

The analysis results for trace elements are shown in Table 3. The total amount of rare earth elements varies greatly, with ΣREE ranging from 33.47 × 10^{-6} to 277.81 × 10^{-6} (average 137.09 × 10^{-6}). LREE/HREE varies from 5.97 to 13.82 (average 11.02), and La/Yb changes from 6.25 to 31.71 (average 21.31), showing the characteristic of enrichment of LREE, depletion of HREE, and obvious fractionation of LREE and HREE. δEu varies from 0.72 to 1.25 (average 0.93), and δCe changes from 0.94 to 0.96 (average 0.95), both of which are close to 1, indicating that Ce and Eu anomalies are not obvious. The chondrite standard curve of REE (Figure 10A) reveals the enrichment of LREE and right-leaning patterns.

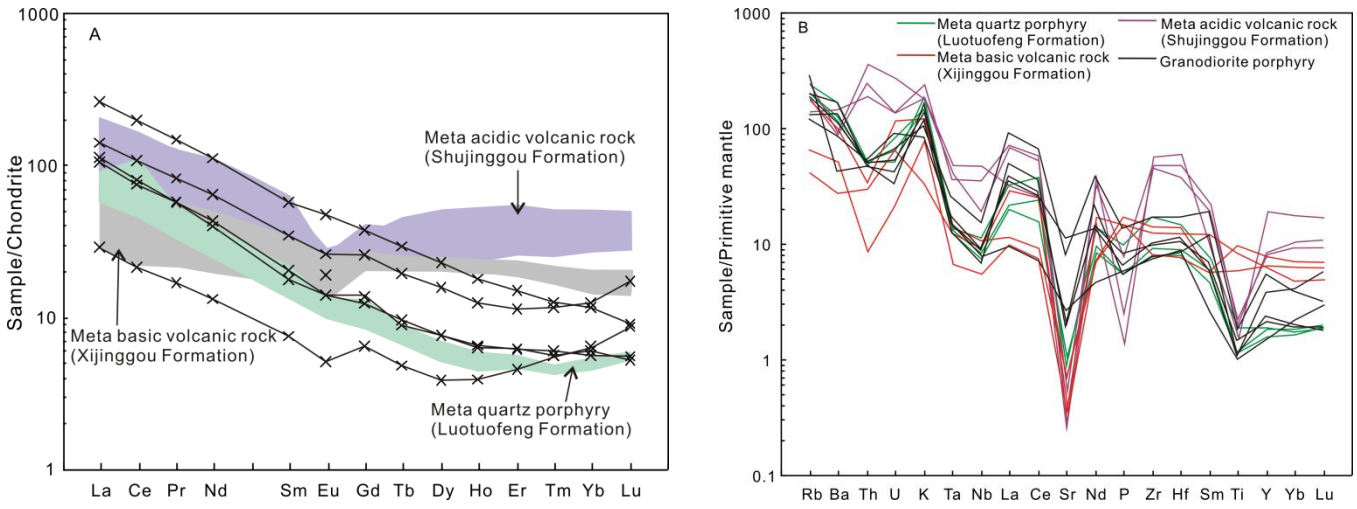

Figure 10. Chondrite-normalized REE patterns diagram (**A**) and primitive mantle normalized trace element spider diagram (**B**) for Tongkuangyu granodiorite porphyry (normalization data after Sun and McDonough, 1989 [53]; regional rock data source as same as Figure 9).

The spider diagram of trace elements is right-leaning (Figure 10B). They are generally enriched in large ion lithophile elements (LILE) (K, Rb, and Ba), light rare earth elements (LREE) (La, Ce), and high field strength elements (HFSE) (Zr, Hf) but depleted in LILE (Th, U) and HFSE (P, Ti). Moreover, they exhibit obvious Nb and Ta negative anomalies, with low Nb/Ta (average 9.8) and Zr/Hf (average 33.9). The loss of P may be related to hydrothermal fluid activity. The loss of Ti may indicate the residual phase of the rutile mineral in the source region. No obvious Eu anomaly is observed (δEu average = 0.95), but a variable Sr negative anomaly is present, which can be interpreted as a reflection of the hydrothermal fluid.

5.3. Zircon Hf Isotopic Compositions

On the basis of zircon U–Pb dating, the in situ Hf isotope analysis of zircon in Tongkuangyu granodiorite porphyry was performed and the results are shown in Table 4. The results show that the ratio of $^{176}Hf/^{177}Hf$ ranges from 0.281368 to 0.281518, the ratio of $^{176}Yb/^{177}Hf$ changes from 0.036421 to 0.064033, the ratio of $^{176}Lu/^{177}Hf$ varies from 0.001058 to 0.001868 and is less than 0.002, indicating that zircons have little accumulation of radioactive genetic Hf isotopes after formation, thus the initial $^{176}Hf/^{177}Hf$ ratio can be used to represent the Hf isotopic composition of the system when the rock formed [54–57]. The $f_{Lu/Hf}$ of all zircons is between −0.97 and −0.94 (average −0.95), ε_{Hf} (t) is from −3.85 to 1.13 (average −1.87). The single-stage mode age (t_{DM1}) is 2462 to 2663 Ma (average 2596 Ma), and two-stage mode age (t_{DM2}) is 2778 to 2959 Ma (average 2849 Ma).

Table 4. Lu–Hf isotopic data of zircons from Tongkuangyu granodiorite porphyry.

Sample No.	t/Ma	$^{176}Hf/^{177}Hf$	2σ	$^{176}Lu/^{177}Hf$	2σ	$^{176}Yb/^{177}Hf$	2σ	ε_{Hf} (t)	2σ	TDM1	TDM2	$f_{Lu/Hf}$
D1-2	2122	0.281439	0.000019	0.001520	0.000028	0.053233	0.001110	−1.86	0.68	2567	2824	−0.95
D1-3	2150	0.281368	0.000015	0.001058	0.000021	0.036421	0.000678	−3.12	0.53	2634	2922	−0.97
D1-4	2143	0.281379	0.000023	0.001705	0.000039	0.053008	0.000834	−3.80	0.82	2663	2959	−0.95
D1-5	2146	0.281422	0.000017	0.001868	0.000031	0.061068	0.000435	−2.46	0.60	2616	2879	−0.94
D1-6	2176	0.281443	0.000016	0.001698	0.000020	0.058920	0.000709	−0.81	0.58	2574	2800	−0.95
D1-9	2169	0.281390	0.000022	0.001856	0.000006	0.064033	0.000249	−3.08	0.78	2659	2934	−0.94
D1-10	2173	0.281429	0.000017	0.001388	0.000006	0.048732	0.000257	−0.91	0.59	2572	2805	−0.96
D1-12	2184	0.281435	0.000018	0.001300	0.000010	0.043695	0.000366	−0.34	0.62	2559	2778	−0.96
D1-16	2135	0.281518	0.000018	0.001590	0.000005	0.054155	0.000303	1.13	0.65	2462	2650	−0.95
D1-18	2121	0.281379	0.000020	0.001407	0.000011	0.046334	0.000420	−3.85	0.72	2642	2945	−0.96
D1-19	2184	0.281413	0.000020	0.001566	0.000021	0.053001	0.000908	−1.50	0.72	2607	2849	−0.95

6. Discussion

6.1. Tempo of Porphyry Intrusion

A number of chronological studies have been carried out by researchers on the porphyry body and surrounding rock of the Tongkuangyu deposit, but the results are quite different due to the different isotopic dating methods. Early scholars mainly used the K–Ar dating method to date the age of the biotite, muscovite, and other minerals from the ore body and host rock, and ages ranged from 694 to 1932 Ma [1]. The K–Ar isotopic system is susceptible to later metamorphic events and thermal activities because of low closure temperature and thus the measured age does not represent the true age of the rock formation and may represent the age of the metamorphic events or thermal activities.

In recent years, high precision zircon U-Pb methods have been used to determine the diagenetic age of the ore-hosting rock. Zhao (2006) [23] used the SHRIMP zircon U-Pb to measure the age of the metamorphic rhyolite of the Tongkuangyu sub-group and came up with a figure of 2273 ± 18 Ma. Li et al. (2008) [58] used LA-ICP MS zircon U-Pb to date the detrital zircons of the Jiangxian Group and obtained an age of 2160 to 2290 Ma. Zhang (2012) [34] used LA-ICP MS zircon U-Pb to determine the age of the tuff in the Tongkuangyu sub-group and found it to be 2198.6 ± 4.7 Ma while the age of metamorphic rhyolitic tuff was estimated at 2160.5 ± 7.8 Ma. Liu et al. (2015) [29] used SIMS zircon U-Pb to measure the age of amphibolite in the interlayer of the Jiangxian Group and came up with an age of 2189 Ma. Yang et al. (2015) [52] obtained the formation age (2179 ± 7 Ma) of the Luotuofeng Formation in the Tongkuangyu sub-group using the SHRIMP zircon U-Pb and that of the Shujinggou Formation was 2142 ± 11 Ma. Combined with previous dating, the volcanic rocks of the Tongkuangyu sub-group may have been formed between 2140 and 2200 Ma.

The age restricting of the ore-forming porphyry body has also been carried out. Xu et al. (2012) [59] used LA–ICP MS zircon U–Pb to measure the age of the ore-forming granite porphyry body, finding that it was from 2128 to 2163 Ma. In addition, a single age of

2121 ± 10 Ma (2σ, MSWD = 1.3) was reported by Li et al. (2013) [60] for a granodiorite porphyry sample, but no location was provided and we have not been able to replicate this result. In this study, the diagenetic age of metallogenic granodiorite porphyry obtained by LA–ICP MS zircon U–Pb is 2159 ± 19 Ma, which is consistent with the age of the ore-forming rock in the ore district. This indicates that the ore-forming rock body that intruded into the Tongkuangyu sub-group may have been formed between 2120 and 2160 Ma, which is a little later than the volcanic rock of the Tongkuangyu sub-group.

6.2. Source Characteristics

Zircon Hf isotopes have been widely used in the study of the source materials and characteristics of granite. Granitic rock with positive $\varepsilon_{Hf}(t)$ values generally comes from the partial melting of depleted mantle or newly accreted crust from depleted mantle, while granitic rock with negative $\varepsilon_{Hf}(t)$ values generally comes from crustal materials. The $\varepsilon_{Hf}(t)$ values of Tongkuangyu granodiorite porphyry are −3.8 to 1.13, most of which are negative and a small part of which are positive, indicating that in addition to crustal material, mantle material might also be incorporated in the magma source. The two-stage model ages (t_{DM2}) range from 2778 to 2959 Ma with an average of 2849 Ma. In the diagram of ε_{Hf} (t) − t (Figure 11), all data fall below the depleted mantle evolution curve and on the 2.7 Ga crust evolution curve. Liu et al. (2012) [28] revealed two major periods of crustal growth in Zhongtiaoshan, i.e., ~3.8 Ga and ~2.7 Ga, by using detrital zircon U-Pb and Lu-Hf analyses. Zhu et al. (2013) [25] discovered 2.7 Ga TTGs and diorite in later research. Liu et al. (2016b) [61] suggested that porphyry magmas were likely sourced from the melting of 2.7 Ga diorite using zircon U-Pb, Hf, and oxygen isotope analyses. It is worth mentioning that in a previous SIMS U-Pb study, an inherited zircon grain with a $^{207}Pb/^{206}Pb$ age of ~2720 was discovered in ore-forming porphyry [29]. Therefore, the initial materials of the Tongkuangyu granodiorite porphyry mainly originated from the Archean continental crust (~2.7 Ga) that involved some mantle components.

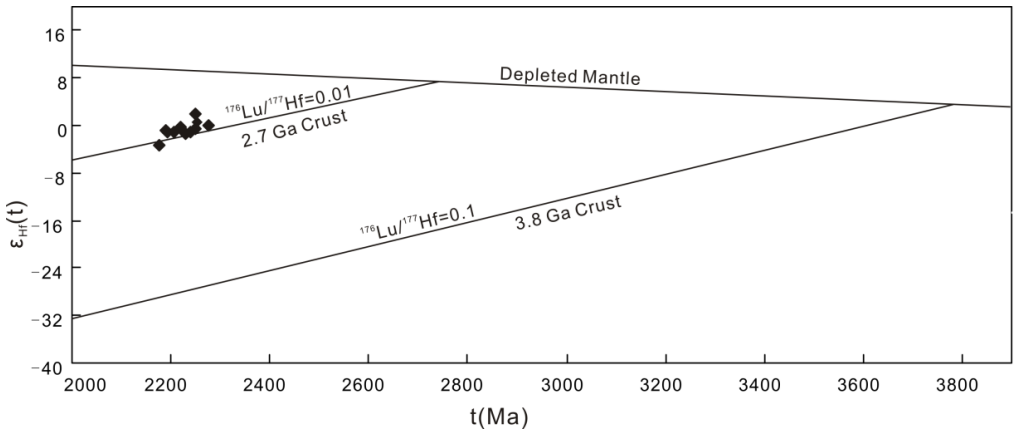

Figure 11. Diagram of zircon $\varepsilon_{Hf}(t)$ values vs. U-Pb ages for granodiorite porphyries at Tongkuangyu Cu deposit (2.7 Ga and 3.8 Ga crust lines were constructed through 2.7 Ga diorite [25] and Songjiashan Formation (detrital zircon) [28] assuming a $^{176}Lu/^{177}Hf$ ratio of 0.01).

6.3. Petrogenesis

The ignition loss of the Tongkuangyu granodiorite porphyry varies from 1.49% to 2.68%, reflecting that it may have experienced a certain degree of late alteration, but the content and ratio of strong incompatible elements (Zr, Nb, Ce, Pb, U, etc.) is relatively stable, which can be used to trace its source property and rock origin.

Geochemically, the Tongkuangyu granite porphyries exhibit several unique features: (1) sodium-rich, large La/Yb ratios, no Eu anomaly, Nb–Ta–Ti negative anomaly, resembling Archean TTG [62]; (2) elevated concentrations of K, Mg, resembling sanukitoid [63]. As mentioned above, porphyry magmas were likely sourced from the melting of 2.7 Ga diorite.

In order to further verify whether partial melting of 2.7 Ga diorite is capable of yielding the geochemical characteristics of the Tongkuangyu granodiorite porphyry, three geochemical factors are considered, including Eu anomaly, K content, and La/Yb ratio. The absence of the Eu anomaly of porphyry magmas implicitly reflects the absence of plagioclase in the source residue.

In terms of K content, mass balance estimates indicate that the partial melting of all feldspar and quartz will produce melts with K content of about 3.3 wt.%, implying that partial melting of diorite is capable of elevating the K content of the resulting melts. Meanwhile, Zhu et al. (2013) [25] considered that 2.7 Ga diorite mainly included amphibole (25% vol.), plagioclase (45% vol.), K-feldspar (10% vol.), biotite (6% vol.), quartz (5% vol.), and other minerals (9% vol.) in mineral compositions. Therefore, elevated concentrations of K in porphyry may be related to the partial melting of diorite.

In addition, the Tongkuangyu granite porphyry is characterized by a lower Yb and a higher La/Yb. Magma melting experiments show that melt model with plagioclase as residual phase has higher Yb and La/Yb but when garnet appears in the residual phase Yb content in the melt decreases but the La/Yb ratio increases rapidly. Through calculation, it is found that when the partial melting degree of 2.7 Ga diorite is 40–80%, with 75% amphibole and 25% biotite as the residual phase, or partial melting degree is 5–50%, with 40% amphibole and 60% biotite as the residual phase, a melt model with a lower Yb and a higher La/Yb will be generated [61], which is roughly similar to the REE model of the Tongkuangyu granodiorite porphyry.

6.4. Tectonic Evolution

There exist different views on the tectonic setting of Zhongtiaoshan in the Paleoproterozoic [31,64,65]. One view is that the Trans-North China Orogen (including Zhongtiaoshan at its southern margin) was built on the Neoarchean continental block and experienced a westward lithospheric subduction ~2170–2120 Ma [30]. Zhao et al. (2001, 2005, 2012) [18,65,66] and Zhao and Zhai (2013) [31] believe that the Trans-North China Orogen belonged to the active continental margin of the Eastern Block underneath the oceanic subduction before 1.85 Ga. Li et al. (2009) [67] and Liu et al. (2012) [28] consider that the Jiangxian Group was formed in the back-arc basin. By contrast, another view is that Zhongtiaoshan was in intracontinental rift environment ~2300–1950 Ma [15,68,69], which is also supported by tectonic and geochemical studies [1,29,70,71].

However, no real arc-derived rocks in the Paleoproterozoic have been discovered in this area to date, but bimodal volcanic rocks (Shujinggou meta-rhyolite and Xijinggou meta-basic volcanic rocks) are relatively developed, which is thought to have been formed in the continental rift basin [23,28]. In addition, Xue (2006) [71] also proved that rock assemblages of the Tongkuangyu sub-group represent the transition from continental sedimentation (possibly red beds) to marine volcanism, indicating a thermal and oxidized environment on the surface and a gradual opening of the rift basin, accompanied by the generation of bimodal volcanic rocks.

Our study also shows that Tongkuangyu granodiorite porphyry has similar geochemical characteristics to those of bimodal volcanic rocks (Shujinggou meta-rhyolite and Xijinggou meta-basic volcanic rocks). Meanwhile, the residual mineral assemblage of biotite for the Tongkuangyu granodiorite porphyry also indicates that it was formed in a relatively low-pressure environment, which may reflect intracontinental rift environment tectonicically.

On the Nb–Y tectonic discrimination diagram (Figure 12A), the samples fall into volcanic arc granite and syn–collisional granite and close to the intraplate granite area. On the Ta–Yb tectonic discrimination diagram (Figure 12B), the samples fall into volcanic arc area and some of them fall into the post-collision area. The LILEs of the Tongkuangyu granodiorite porphyry are enriched in K, Rb, and Ba, but depleted in U and Th, and the HFSEs are also enriched in Zr and Hf, but depleted in Nb, Ta, P, and Ti, exhibiting different geochemical characteristics from those of typical volcanic arc granites. These results imply that a plate subduction event may have occurred in the Zhongtiaoshan area before the

formation of the Tongkuangyu granodiorite porphyry (~2160 Ma), which affected the formation of granodiorite porphyry and retained the effect of the plate subduction.

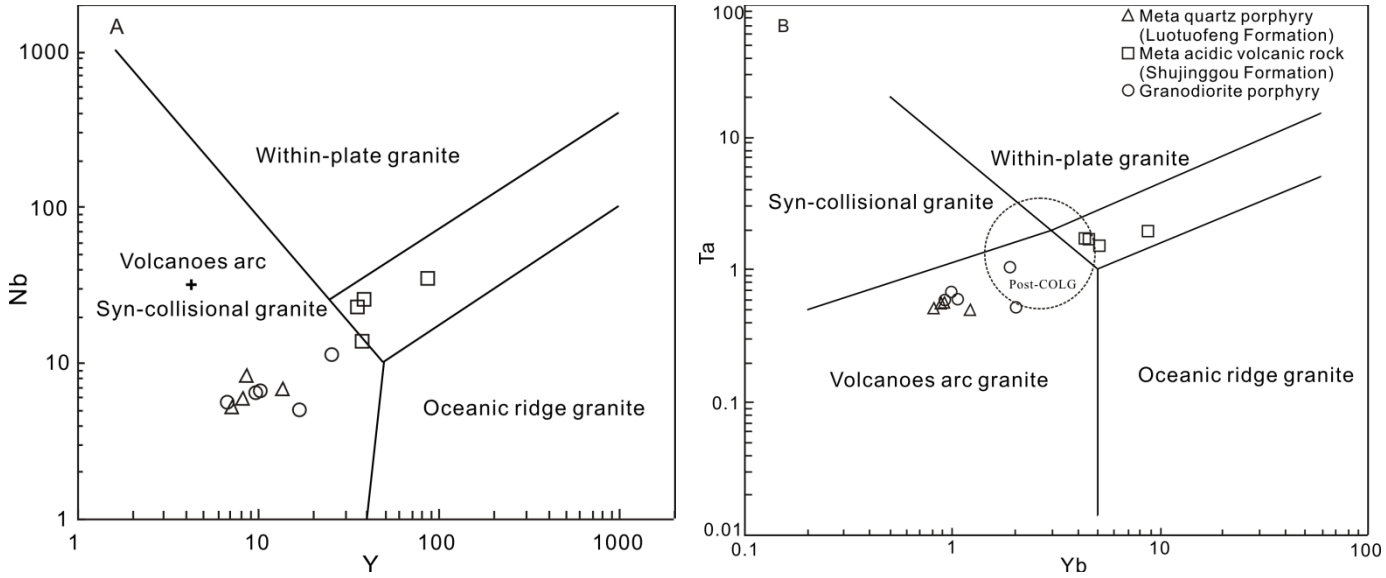

Figure 12. Y vs. Nb (**A**) and Yb vs. Ta (**B**) diagrams of Tongkuangyu granodiorite porphyry (after Pearce et al., 1984 [72]; regional rock data source as same as Figure 9).

Liu et al. (2016) [61] proposed that oceanic crust subduction occurred at ~2.7 Ga, followed by a continental collision at ~2.5 Ga, which ended up in the Zhongtiaoshan area at ~2.2 Ga. After that, the crustal rifting at ~2.1 Ga and the Zhongtiao collisional orogeny at ~1.8 Ga occurred, which are interpreted as representing the Jiangxian movement and Zhongtiao orogeny [13,20]. Therefore, we propose that, after ~2.2 Ga, the early thickened crust was significantly thinned by lithospheric extension and the tectonic environment also transformed from early subduction orogeny to post-orogenic extension. Due to the extension and thinning of the crust, the underplating of the mantle-derived basaltic magma occurred during this period, causing partial melting of 2.7 Ga diorite and forming rhyolitic magma, causing crust–mantle interaction to take place. When these melts erupted to the crustal surface, they formed the bimodal volcanic rocks of the Xijinggou and Shujinggou Formations. When felsic and basaltic magmas mixed, they became parental magmas for the Tongkuangyu granodiorite porphyry.

7. Conclusions

The Tongkuangyu granodiorite porphyry shows geochemical affinities to both Archean TTG and sanukitoid. Geochemical modeling suggests that melts produced by the remelting of the 2.7 Ga diorite can achieve similar geochemical features to those of Tongkuangyu porphyry. Furthermore, zircon Hf isotopes indicate that the Tongkuangyu granodiorite porphyry is mainly derived from partial melting of the Archean crust (~2.7 Ga), with a little mantle-derived material added. Zircon U-Pb dating suggests that the Tongkuangyu porphyry formed at ~2160 Ma, which is broadly coeval with ore formation (~2.1 Ga) in the area. The Tongkuangyu granodiorite porphyry may have been formed in the tectonic environment of post-orogenic extension, and the Tongkuangyu Cu deposit may be a porphyry deposit related to the extension of the North China Craton in the Paleoproterozoic.

Author Contributions: J.S., T.L. and H.L. made field investigation. J.S. performed the zircon U–Pb dating and Lu–Hf isotope analysis, interpreted all the data and finished the original draft of the paper. H.L. reviewed the original draft of paper and acted as the project administration. K.Y. and Z.W. provided the geological maps and performed the whole-rock geochemical analysis. Y.C. corrected the language. All authors have read and agreed to the published version of the manuscript.

Funding: This study was financially supported by the National Natural Science Foundation of China (41602074, 41430314) and the Project of China Geological Survey (DD20190606, DD20211574, DD20221686).

Data Availability Statement: The data used to support the findings of this study are available from the corresponding author upon request.

Acknowledgments: We would like to thank the Geophysical and Chemical Exploration Institute of Shanxi Province for their full support for field work. We are grateful to Kejun Hou and Chunli Guo, from the Institute of Mineral Resources of the Chinese Academy of Geological Sciences, for their important guidance and assistance in the zircon age testing, Hf isotope testing, and data analysis. Thanks to the anonymous reviewer for valuable comments and suggestions.

Conflicts of Interest: The authors declare no conflict of interest.

References

1. Compilation Group of Geology of the Copper Deposits in Zhongtiao Mountain (CGGCDZM). *Geology of the Copper Deposits in Zhongtiao Mountain*; Geological Publishing House: Beijing, China, 1978; pp. 25–86. (In Chinese)
2. Jiang, Y.; Niu, H.; Bao, Z.; Li, N.; Shan, Q.; Yang, W. Fluid evolution of the Tongkuangyu porphyry copper deposit in the Zhongtiaoshan region: Evidence from fluid inclusions. *Ore Geol. Rev.* **2014**, *63*, 498–509. [CrossRef]
3. Jiang, Y.; Niu, H.; Bao, Z.; Li, N.; Shan, Q.; Yang, W.; Yan, S. Fluid evolution of the Paleoproterozoic Hujiayu copper deposit in the Zhongtiaoshan region: Evidence from fluid inclusions and carbon–oxygen isotopes. *Precambrian Res.* **2014**, *255*, 734–747. [CrossRef]
4. Sun, J.G.; Li, H.Y.; Liu, X.H.; Xie, K.Q.; Li, B.L.; Yin, D.W. Alteration and mineralization characteristics of Tongkuangyu copper deposit in Zhongtiao Mountain, Shanxi Province. *Miner. Depos.* **2014**, *33*, 1306–1324, (In Chinese with English Abstract).
5. Sun, J.G.; Li, H.Y.; Liu, X.H.; Xie, K.Q.; Chen, W.; Xue, S.S.; Sun, X.L. Characteristics of chlorite from the Tongkuangyu copper deposit in Shanxi Province and their geological implications. *Bull. Mineral. Petrol. Geochem.* **2015**, *34*, 1142–1154, (In Chinese with English Abstract).
6. Sun, J.G. Geological Characteristics and Genesis of the Tongkuangyu copper Deposit in Zhongtiao Mountain, Shanxi Province. Master's Thesis, China University of Geosciences in Beijing, Beijing, China, 2015.
7. Li, H.Y.; Luo, W.J.; Sun, J.G.; Yang, L.; Xie, K.Q.; Zhou, X.P.; Xue, S.S.; Yin, D.W.; Guo, S.L.; Zhao, F.C.; et al. Characteristics of ore-forming fluids of Tongkuangyu porphyry copper deposit in Zhongtiao Mountain, Shanxi Province. *Miner. Depos.* **2018**, *37*, 1091–1110, (In Chinese with English Abstract).
8. Meng, X.; Richards, J.; Mao, J.; Ye, H.; DuFrane, S.A.; Creaser, R.; Marsh, J.; Petrus, J. The Tongkuangyu Cu deposit, trans-north china orogen: A metamorphosed paleoproterozoic porphyry Cu deposit. *Econ. Geol.* **2020**, *115*, 51–77. [CrossRef]
9. Zhou, X. Studies on Geological-Geochemical Characteristics of Tongkuangyu Iron Oxide-Copper-Gold Deposit in Zhongtiao Mountains, Shanxi Province. Master's Thesis, Central South University, Changsha, China, 2007.
10. Sun, H.T.; Ge, C.H.; Ji, S.K. Isotopic ages of precambran strata in the Zhongtiao mountains area and their significance. *Reg. Geol. China* **1990**, *3*, 237–248, (In Chinese with English Abstract).
11. Xie, J.R. Problems pertaining to geology and ore deposits of a copper deposit in shanxi province. *Sci. China Ser. A* **1963**, *9*, 1345–1355.
12. Liu, X.; Fan, H.R.; Santosh, M.; Yang, K.F.; Qiu, Z.J.; Hu, F.F.; Wen, B.J. Geological and geochronological constraints on the genesis of the giant Tongkuangyu Cu deposit (Palaeoproterozoic), North China Craton. *Int. Geol. Rev.* **2016**, *58*, 155–170. [CrossRef]
13. Mei, H.L. Metamorphic P-T-t paths and tectonic evolution of early Proterozoic rocks from the Zhongtiao Mountains, Southern Shanxi. *Geol. Rev.* **1994**, *40*, 36–47, (In Chinese with English Abstract).
14. Sun, D.Z.; Li, H.M.; Lin, Y.X.; Zhou, H.F.; Zhao, F.Q.; Tang, M. Precambrian geochronology, chronotectonic framework and model of chronocrustal structure of the Zhongtiao Mountain. *Acta Geol. Sin.* **1991**, *3*, 216–231, (In Chinese with English Abstract).
15. Zhai, M.G.; Liu, W. Paleoproterozoic tectonic history of the North China Craton: A review. *Precambrian Res.* **2003**, *122*, 183–199. [CrossRef]
16. Zhao, G.C.; Wilde, S.A.; Guo, J.H.; Cawood, P.A.; Sun, M.; Li, X.P. Single zircon grains record two Paleoproterozoic collisional events in the North China Craton. *Precambrian Res.* **2010**, *177*, 266–276. [CrossRef]
17. Zhang, J.; Zhao, G.C.; Li, S.Z.; Sun, M.; Wilde, S.A.; Liu, S.W.; Yin, C.Q. Polyphase deformation of the Fuping Complex, Trans-North China orogen: Structures, SHRIMP U-Pb zircon ages and tectonic implications. *J. Struct. Geol.* **2009**, *31*, 177–193. [CrossRef]
18. Zhao, G.C.; Sun, M.; Wilde, S.A.; Li, S.Z. Late archean to paleoproterozoic evolution of the North China Craton: Key issues revisited. *Precambrian Res.* **2005**, *136*, 177–202. [CrossRef]
19. Zhao, G.C.; Wilde, S.A.; Sun, M.; Li, S.Z.; Li, X.P.; Zhang, J. SHRIMP U-Pb zircon ages of granitoid rocks in the Lüliang Complex: Implications for the accretion and evolution of the Trans-North China orogen. *Precambrian Res.* **2008**, *160*, 213–226. [CrossRef]
20. Sun, D.Z.; Hu, W.X. *Precambrian Chronotectonic Framework and Model of Chronocrustal Structure of the Zhongtiao Mountains*; Geological Publishing House: Beijing, China, 1993; pp. 88–96. (In Chinese)

21. Sun, D.Z.; Hu, W.X.; Tang, M.; Zhao, F.Q.; Condie, K.C. Origin of late archean and early proterozoic rocks and associated mineral deposits from the Zhongtiao Mountains, east-central China. *Precambrian Res.* **1990**, *47*, 287–306.
22. Tian, W.; Liu, S.W.; Zhang, H.F. Paleoproterozoic potassic granitoids in the Sushui Complex from the Zhongtiao mountains, Northern China. Geochronology, geochemistry and petrogenesis. *Acta Geol. Sin. (Engl. Ed.)* **2006**, *80*, 875–885.
23. Zhao, F.Q. Geochronologic and Geochemical Constraints on the Paleoproterozoic Crustal Evolution of Zhongtiao Mountains from Shanxi Province. Ph.D. Thesis, China University of Geosciences in Beijing, Beijing, China, 2006.
24. Guo, L.S.; Liu, S.W.; Liu, Y.L.; Tian, W.; Yu, S.Q.; Li, Q.G.; Lyu, Y.J. Zircon Hf isotopic features of TTG gneisses and formation environment of Precambrian Sushui complex in Zhong tiao mountains. *Acta Petrol. Sin.* **2008**, *24*, 139–148.
25. Zhu, X.Y.; Zhai, M.G.; Chen, F.K.; Lyu, B.; Wang, W.; Peng, P.; Hu, B. ~2.7 Ga crustal growth in the North China Craton: Evidence from zircon U-Pb Ages and Hf isotopes of the Sushui Complex in the Zhongtiao terrane. *J. Geol.* **2013**, *121*, 239–254. [CrossRef]
26. Zhang, R.Y.; Zhang, C.L.; Diwu, C.R.; Sun, Y. Zircon U-Pb geochronology, geochemistry and its geological implications for the Precambrian granitoids in Zhongtiao Mountain, Shanxi Province. *Acta Petrol. Sin.* **2012**, *28*, 3559–3573.
27. Li, Q.G.; Liu, S.W.; Wang, Z.Q.; Shen, Y.; Zhang, L.; Zhang, J. Provenance and geotectonic setting of the Palaeoproterozoic Zhongtiao Group and implications for assembly of the North China Craton: Whole-rock geochemistry and detrital zircon data. *J. Geol. Soc.* **2011**, *168*, 1215–1224. [CrossRef]
28. Liu, C.H.; Zhao, G.C.; Sun, M.; Zhang, J.; Yin, C. U–Pb geochronology and Hf isotope geochemistry of detrital zircons from the Zhongtiao Complex: Constraints on the tectonic evolution of the Trans-North China orogen. *Precambrian Res.* **2012**, *222*, 159–172. [CrossRef]
29. Liu, X.; Fan, H.R.; Qiu, Z.J.; Yang, K.F.; Hu, F.F.; Wen, B.J. Formation ages of the Jiangxian and Zhongtiao groups in the Zhongtiao Mountain region, North China Craton: Insights from SIMS U-Pb dating on zircons from intercalated plagioclase amphibolites. *Acta Petrol. Sin.* **2015**, *6*, 1564–1572, (In Chinese with English Abstract).
30. Faure, M.; Trap, P.; Lin, W.; Monié, P.; Bruguier, O. Polyorogenic evolution of the paleoproterozoic Trans–North China belt–new insights from the Luliangshan–Hengshan–Wutaishan and Fuping massifs. *Episodes* **2007**, *30*, 95–106. [CrossRef]
31. Zhao, G.C.; Zhai, M.G. Lithotectonic elements of Precambrian basement in the North China Craton: Review and tectonic implications. *Gondwana Res.* **2013**, *23*, 1207–1240. [CrossRef]
32. Zhai, M.G.; Santosh, M. Metallogeny of the North China Craton: Link with secular changes in the evolving Earth. *Gondwana Res.* **2013**, *24*, 275–297. [CrossRef]
33. Zhao, T.P.; Zhai, M.G.; Xia, B.; Li, H.M.; Zhang, Y.X.; Wan, Y.S. Zircon U-Pb SHRIMP dating for the volcanic rocks of the Xiong'er group: Constraints on the initial formation age of the cover of the North China Craton. *Chin. Sci. Bull.* **2004**, *49*, 2495–2502. [CrossRef]
34. Zhang, H. Metallogenesis of Paleoproterozoic copper Deposits in the Northern Zhongtiaoshan Mountains, Shanxi Province. Ph.D. Thesis, Jilin University, Jilin, China, 2012.
35. Xu, Q.L. Study on the Geological Characteristics and Ore Genesis of Tongkuangyu copper Deposit in the Zhongtiaoshan Moubtains, Shanxi Province. Master's Thesis, Jilin University, Jilin, China, 2012.
36. Chen, Z.H.; Yang, Y.C.; Han, S.J.; Zhang, G.B. Geochemical characteristics of ore-bearing rock series and ore genesis of Tongkuangyu copper deposit in Zhongtiao mountains. *Glob. Geol.* **2014**, *33*, 348–357, (In Chinese with English Abstract).
37. Chen, W.M.; Zhang, C.X.; Lu, J.R.; Dang, Z.F.; Li, S.B.; Cui, W.B.; Ning, Y.; Cao, Y.J. Ore-hosted rock of the Zhongtiaoshan metamorphic porphyry copper deposit and its recovery. *Miner. Depos.* **1998**, *17*, 523–526, (In Chinese with English Abstract).
38. Sun, J.Y.; Ji, S.K.; Zhen, Y.Q. *The Copper Deposits in the Zhongtiao Rift*; Geological Publishing House: Beijing, China, 1995; pp. 1–194, (In Chinese with English Abstract).
39. Liu, Y.S.; Hu, Z.C.; Gao, S. In situ analysis of major and trace elements of anhydrous minerals by LA–ICP–MS without applying an internal standard. *Chem. Geol.* **2008**, *257*, 34–43. [CrossRef]
40. Ludwing, K.R. *User's Manual for Isoplot 3.00: A Geochronological Toolkit for Microsoft Excel*; Berkeley Geochronology Center (Special Publication): Berkeley, CA, USA, 2003; pp. 1–74.
41. Hou, K.J.; Li, Y.H.; Tian, Y.R. In situ U–Pb zircon dating using laser ablation–multion counting ICP–MS. *Miner. Depos.* **2009**, *28*, 481–492, (In Chinese with English Abstract).
42. Hou, K.J.; Li, Y.H.; Zou, T.R.; Qu, X.M.; Shi, Y.R.; Xie, G.Q. Laser ablation MC–ICP–MS technique for Hf isotope microanalysis of zircon and its geological application. *Acta Petrol. Sin.* **2007**, *23*, 2595–2604, (In Chinese with English Abstract).
43. Wu, F.Y.; Yang, Y.H.; Xie, L.W. Hf isotopic compsitions of the standard zircons and baddeleyites used in U–Pb geochronology. *Chem. Geol.* **2006**, *234*, 105–126. [CrossRef]
44. Soderlund, U.; Patchett, P.J.; Vervoort, J.D.; Isachsen, C.E. The176Lu decay constant determined by Lu–Hf and U–Pb isotope systematics of Precambrian mafic intrusions. *Earth Planet. Sci. Lett.* **2004**, *219*, 311–324. [CrossRef]
45. Blichert-Toft, J.; Albarède, F. The Lu–Hf isotope geochemistry of chondrites and the evolution of the mantle–crust system. *Earth Planet. Sci. Lett.* **1997**, *148*, 243–258. [CrossRef]
46. Griffin, W.L.; Pearson, N.J.; Belousova, E.; Jackson, S.E.; Van Achterbergh, E.; O'Reilly, S.Y.; Shee, S.R. The Hf isotope composition of cratonic mantle: LA–MC–ICP MS analysis of zircon megacrysts in kimberlites. *Geochim. Cosmochim. Acta* **2000**, *64*, 133–147. [CrossRef]

47. Veevers, J.J.; Saeed, A.; Belousova, E.A.; Griffin, W.L. U–Pb ages and source composition by Hf–isotope and trace–element analysis of detrital zircons in Permian sandstone and modern sand from southwestern Australia and a review of the paleogeographical and denudational history of the Yilgarn Craton. *Earth Sci. Rev.* **2005**, *68*, 245–279. [CrossRef]
48. Winchester, J.A.; Floyd, P.A. Geochemical discrimination of different magma series and their differentiation products using immobile elements. *Chem. Geol.* **1977**, *20*, 325–343. [CrossRef]
49. Middlemost, E.A.K. *Magmas and Magmatic Rocks*; Longman: London, UK, 1985; pp. 258–266.
50. Middlemost, E.A.K. Naming materials in the magma/igneous rock system. *Earth Sci. Rev.* **1994**, *37*, 215–224. [CrossRef]
51. Peccerillo, R.; Taylor, S.R. Geochemistry of eocene calc–alkaline volcanic rocks from the Kastamonu area, Northern Turkey. *Contrib. Mineral. Petrol.* **1976**, *58*, 63–81. [CrossRef]
52. Yang, C.H.; Du, L.L.; Ren, L.D.; Song, H.X.; Geng, Y.S.; Wang, Y.B.; Lu, Z.L.; Wang, H.; Li, Y.H. The age and tectonic setting of metavolcanic rocks in the Tongkuangyu deposit, Zhongtiao Mountain, and their constraints on copper mineralization. *Acta Geosci. Sin.* **2015**, *36*, 613–633, (In Chinese with English Abstract).
53. Sun, S.S.; McDonough, W.F. Chemical and isotopic systematics and oceanic basalts: Implication for mantle composition and processes. In *Magmatism in the Ocean Basins*; Saunders, A.D., Norry, M.J., Eds.; Geological Society Special Publication: London, UK, 1989; Volume 42, pp. 313–345.
54. Patchett, P.J.; Kouvo, O.; Hedge, C.E.; Tatsumoto, M. Evolution of continental crust and mantle heterogeneity: Evidence from Hf isotope. *Contrib. Mineral. Petrol* **1981**, *78*, 279–297. [CrossRef]
55. Knudsen, T.L.; Griffin, W.L.; Hartz, E.H.; Andresen, A.; Jackson, S. In–situ hafnium and lead isotope analyses of detrital zircons from the Devonian sedimentary basin of NE Greenland: A record of repeated crustal reworking. *Contrib. Mineral. Petrol.* **2001**, *141*, 83–94. [CrossRef]
56. Kinny, P.D.; Maas, R. Lu–Hf and Sm–Nd isotope systems in zircon. *Rev. Mineral. Geochem.* **2003**, *53*, 327–341. [CrossRef]
57. Wu, F.Y.; Li, X.H.; Yang, J.H.; Zheng, Y.F. Discussions on the petrogenesis of granites. *Acta Petrol. Sin.* **2007**, *23*, 1217–1238, (In Chinese with English Abstract).
58. Li, Q.G.; Liu, S.W.; Wang, Z.Q.; Zhang, F.; Chen, Y.Z.; Wang, T. LA-ICPMS U-Pb geochronology of the detrital zircons from the Jiangxian group in the Zhongtiao mountain and its tectonic significance. *Acta Petrol. Sin.* **2008**, *24*, 1359–1368, (In Chinese with English Abstract).
59. Xu, Q.L.; Sun, F.Y.; Zhang, H.; Huo, L. Fluid inclusions, zircon U-Pb age and Hf isotope of Tongkuangyu copper deposit in Zhongtiaoshan mountains and its geological significance, Shanxi Province, China. *J. Jilin Univ. (Earth Sci. Ed.)* **2012**, *42*, 64–80.
60. Li, N.B.; Luo, Y.; Jiang, Y.H.; Guo, S.L.; Niu, H.C. Zircon U–Pb geochronology and Hf isotopic characteristic of metamorphic quartz-monzonite porphyry from Tongkuangyu area, Zhongtiao Mountain and their geological implications. *Acta Petrol. Sin.* **2013**, *29*, 2416–2424, (In Chinese with English Abstract).
61. Liu, X.; Fan, H.R.; Yang, K.F.; Qiu, Z.J.; Hu, F.F.; Zhu, X.Y. Geochronology, redox-state and origin of the ore-hosting porphyry in the Tongkuangyu Cu deposit, North China Craton: Implications for metallogenesis and tectonic evolution. *Precambrian Res.* **2016**, *276*, 211–232. [CrossRef]
62. Moyen, J.F.; Martin, H. Forty years of TTG research. *Lithos* **2012**, *148*, 312–336. [CrossRef]
63. Martin, H.; Moyen, J.F.; Rapp, R. The sanukitoid series: Magmatism at the Archean-Proterozoic transition. *Earth Environ. Sci. Trans. R. Soc. Edinb.* **2010**, *100*, 15–33.
64. Zhai, M.G.; Santosh, M. The early Precambrian odyssey of the North China Craton: A synoptic overview. *Gondwana Res.* **2011**, *20*, 6–25. [CrossRef]
65. Zhao, G.C.; Cawood, P.A.; Li, S.Z.; Wilde, S.A.; Sun, M.; Zhang, J.; He, Y.H.; Yin, C.Q. Amalgamation of the North China Craton: Key issues and discussion. *Precambrian Res.* **2012**, *222–223*, 55–76. [CrossRef]
66. Zhao, G.; Wilde, S.A.; Cawood, P.A.; Sun, M. Archean blocks and their boundaries in the North China Craton: Lithological, geochemical, structural and P-T path constraints and tectonic evolution. *Precambrian Res.* **2001**, *107*, 45–73. [CrossRef]
67. Li, Q.G.; Chen, X.; Liu, S.W.; Wang, Z.Q.; Zhou, Y.K.; Zhang, J.; Wang, T. Evaluating the Provenance of metasedimentary rocks of the Jiangxian Group from the Zhongtiao Mountain using whole-rock geochemistry and detrital zircon Hf isotope. *Acta Geol. Sin.* **2009**, *83*, 550–561. [CrossRef]
68. Zhai, M.G.; Peng, P. Paleoproterozoic events in the North China Craton. *Acta Petrol. Sin.* **2007**, *23*, 2665–2682.
69. Zhai, M.G.; Santosh, M.; Zhang, L.C. Precambrian geology and tectonic evolution of the North China Craton. *Gondwana Res.* **2011**, *20*, 1–5. [CrossRef]
70. Zhen, Y.Q.; Yao, C.F. Stratiform copper deposits within the rift valleys of Zhongtiaoshan area. *J. Guilin Coll. Geol.* **1992**, *12*, 30–40, (In Chinese with English Abstract).
71. Xue, K.Q. Study on the Relation between Structure and Metallogenesis in the Zhongtiao Rift. Ph.D. Thesis, China University of Geosciences (Beijing), Beijing, China, 2006.
72. Pearce, J.A.; Harris, N.B.W.; Tindle, A.G. Trace element discrimination diagrams for the tectonic interpretation of granitic rocks. *J. Petrol.* **1984**, *25*, 956–983. [CrossRef]